TLR9 mediates cellular protection by modulating energy metabolism in cardiomyocytes and neurons

Yasunori Shintani[a,1], Amar Kapoor[a], Masahiro Kaneko[a], Ryszard T. Smolenski[b], Fulvio D'Acquisto[a], Steven R. Coppen[a], Narumi Harada-Shoji[a], Hack Jae Lee[a], Christoph Thiemermann[a], Seiji Takashima[c], Kenta Yashiro[a], and Ken Suzuki[a,1]

[a]William Harvey Research Institute, Barts and The London School of Medicine and Dentistry, Queen Mary University of London, London EC1M 6BQ, United Kingdom; [b]Department of Biochemistry, Medical University of Gdansk, 80-211 Gdansk, Poland; and [c]Department of Molecular Cardiology, Osaka University Graduate School of Medicine, Suita, Osaka 565-0871, Japan

Edited* by Ruslan Medzhitov, Yale University School of Medicine, New Haven, CT, and approved February 15, 2013 (received for review November 6, 2012)

Toll-like receptors (TLRs) are the central players in innate immunity. In particular, TLR9 initiates inflammatory response by recognizing DNA, imported by infection or released from tissue damage. Inflammation is, however, harmful to terminally differentiated organs, such as the heart and brain, with poor regenerative capacity, yet the role of TLR9 in such nonimmune cells, including cardiomyocytes and neurons, is undefined. Here we uncover an unexpected role of TLR9 in energy metabolism and cellular protection in cardiomyocytes and neurons. TLR9 stimulation reduced energy substrates and increased the AMP/ATP ratio, subsequently activating AMP-activated kinase (AMPK), leading to increased stress tolerance against hypoxia in cardiomyocytes without inducing the canonical inflammatory response. Analysis of the expression profiles between cardiomyocytes and macrophages identified that unc93 homolog B1 (*C. elegans*) was a pivotal switch for the distinct TLR9 responses by regulating subcellular localization of TLR9. Furthermore, this alternative TLR9 signaling was also found to operate in differentiated neuronal cells. These data propose an intriguing model that the same ligand–receptor can concomitantly increase the stress tolerance in cardiomyocytes and neurons, whereas immune cells induce inflammation upon tissue injury.

Toll-like receptors (TLRs) were originally identified as receptors for exogenous pathogens, initiating the inflammatory response by immune cells. TLRs initiate downstream signaling to activate the key transcription factor, NF-κB, producing inflammatory cytokines (1). More recently, however, their role in noninfectious insults such as ischemia–reperfusion has been highlighted (2), which is referred to as sterile inflammation. In sterile inflammation, antigen-presenting cells are activated by molecules released from injured self-cells, known as damage-associated molecular patterns (DAMPs), and switch on the inflammatory response. Importantly, TLRs are the major DAMP receptors (3).

Among TLRs, TLR9 is the sole family member for detecting DNA (4). TLR9 was originally found as a sensor for bacterial DNA that has abundant unmethylated CpG dinucleotides (4). However, mammalian DNA of self-origin, which has a low frequency of unmethylated CpG dinucleotides, can also stimulate TLR9. This is strongly underpinned by the recent report showing that TLR9 recognizes the sugar backbone 2′-deoxyribose of DNA, but not its bases, suggesting the nucleotide sequence is not the primary target of TLR9 (5). Therefore, DNA released from damaged cells can trigger sterile inflammation via TLR9, acting as a DAMP (3).

Although it is not surprising that TLR9 is expressed in immune cells, its expression has also been reported in nonimmune cells including cardiomyocytes and neurons (6, 7); yet its relevance in such nonimmune cells is unclear. It would be catastrophic for such organs with poor regenerative capacity, if TLR9 in nonimmune cells operated the same inflammatory signaling. Interestingly, bacterial DNA has recently been shown to decrease contractility in isolated cardiomyocytes within 30 min after administration (8). Although the precise mechanism and biological relevance of this phenomenon remains unknown, we speculated that TLR9 has a different role in cardiomyocytes.

Here we uncover a unique TLR9 signaling pathway that modulates energy metabolism to protect cardiomyocytes and neurons, independent of the canonical inflammatory signaling. Furthermore, our data suggest Unc93b1, a key TLR9-trafficking molecule, is a pivotal switch for the distinct TLR9 responses.

Results

TLR9 Reduces Energy Substrates in Cardiomyocytes with Activation of AMP-Activated Kinase, Leading to Increased Stress Tolerance. First, to confirm the role of TLR9 to reduce contractility, we compared ex vivo crystalloid-perfused, beating hearts from wild-type and TLR9$^{-/-}$ mice using the Langendorff method, which enabled us to eliminate the effect from circulating immune cells. Consistent with the earlier report using isolated cardiomyocytes in vitro (8), CpG oligodeoxynucleotides (CpG-ODN; a synthetic TLR9 ligand) significantly decreased cardiac contractility through TLR9 as early as 20 min following its administration without changing coronary flow (Fig. S1*A*). As nitric oxide and some volatile anesthetics suppress the cardiac contractility with reducing energy metabolism (9), we next measured energy substrates in the heart. Interestingly, the wild-type heart with CpG-ODN showed marked decreases in the ATP/ADP and creatine phosphate/creatine ratios (both of which are indicators for energy metabolism in cardiomyocytes) and an increase in the AMP/ATP ratio (Fig. 1*A*). An increased AMP/ATP ratio is the key trigger for activation of AMP-activated kinase (AMPK) (10, 11). AMPK activation switches off ATP-consuming processes that are not essential for short-term cell survival to increase the cellular tolerance against the metabolic stress (12–14). Indeed, the administration of CpG-ODN increased the phosphorylation of AMPK and its substrate, acetyl-CoA carboxylase (ACC), in the wild-type heart (Fig. 1*B*). Both AMPK activation and the change in energy substrates were completely abrogated in TLR9$^{-/-}$ mice (Fig. 1 *A* and *B*), indicating that the observed metabolic effect was mediated through TLR9.

To further explore whether the AMPK activation observed in the whole heart occurred in cardiomyocytes, we studied primary neonatal cardiomyocytes that also expressed TLR9 (Fig. S1*B*). The increased phosphorylation of AMPK in response to CpG-ODN (type B) was confirmed in these cardiomyocytes, but not in cardiac fibroblasts (a major contaminant of primary cardiomyocyte cultures) (Fig. 1*C*). Type A CpG-ODN also activated AMPK in cardiomyocytes (Fig. 1*C*), indicating that the AMPK activation is independent of CpG-ODN type (CpG-ODN type B was used throughout the remainder of the study). A time-course analysis

Author contributions: Y.S. designed research; Y.S., M.K., A.K., R.T.S., N.H.-S., and H.J.L. performed research; F.D., C.T., and S.T. contributed new reagents/analytic tools; Y.S., F.D., S.R.C., S.T., K.Y., and K.S. analyzed data; and Y.S. and K.S. wrote the paper.

The authors declare no conflict of interest.

*This Direct Submission article had a prearranged editor.

Freely available online through the PNAS open access option.

[1]To whom correspondence may be addressed. E-mail: y.shintani@qmul.ac.uk or ken.suzuki@qmul.ac.uk.

This article contains supporting information online at www.pnas.org/lookup/suppl/doi:10.1073/pnas.1219243110/-/DCSupplemental.

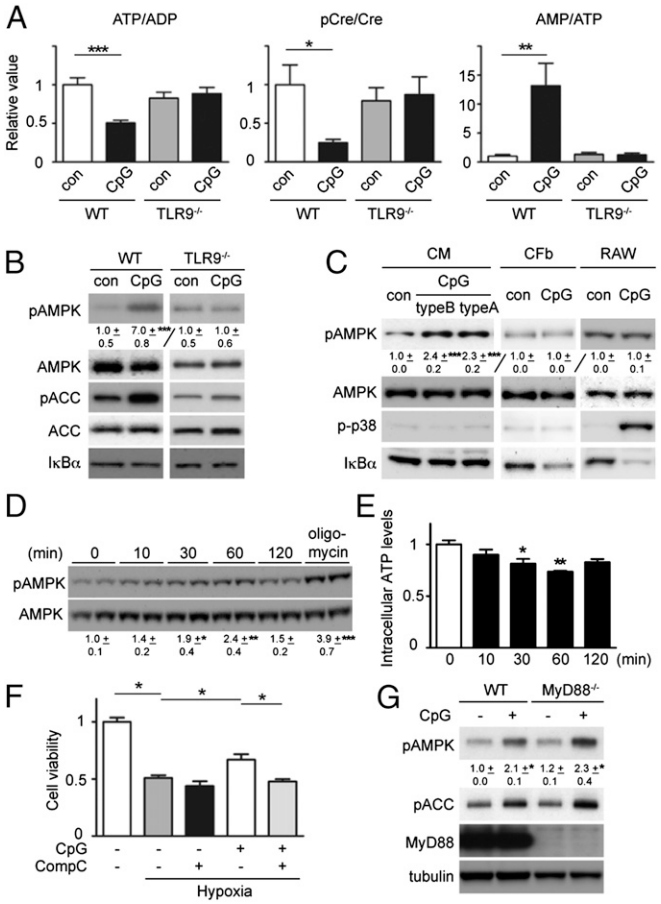

Fig. 1. TLR9 reduces energy substrates with activation of AMPK independent of MyD88, leading to increased stress tolerance in cardiomyocytes. (*A*) Administration of CpG-ODN reduced the level of energy substrates and increased the AMP/ATP ratio in ex vivo perfused heart in wild-type (WT) mice, but not in TLR9$^{-/-}$ mice. The hearts (n = 6 for WT, n = 5 for TLR9$^{-/-}$) were analyzed at 30 min after the administration of CpG-ODN (type B, 0.25 μM) or vehicle (con). (*B*) CpG-ODN increased the phosphorylation of AMPK and its substrate, ACC, without a decrease in IκBα in ex vivo perfused heart in WT mice, but not in TLR9$^{-/-}$ mice. (*C*) CpG-ODN (type B at 3 μM or type A at 1 μM) activated AMPK 60 min after administration in cultured cardiomyocytes (CM), but not in RAW264.7 macrophages (RAW) or in cardiac fibroblasts (CFb). In contrast, the phosphorylation of p38 MAPK and a decrease in IκBα were seen in RAW264.7, but not in cardiomyocytes. The data represent four independent experiments. (*D*) Time-course of AMPK activation by CpG-ODN in cardiomyocytes. Oligomycin A (10 μg/mL for 60 min) was used as a positive control. The data represent two independent experiments. (*E*) The change in intracellular ATP levels in cardiomyocytes treated with CpG-ODN using luminescence-based measurement (n = 3). The data represent two independent experiments. (*F*) Pretreatment with CpG-ODN (30 min before 16 h of hypoxia, n = 6–8) increased the survival of cardiomyocytes against hypoxia. AMPK inhibitor, compound C (1 μM), abrogated the protective effect of CpG-ODN. Cell viability was normalized with normoxia control. The data represent three independent experiments. (*G*) The CpG-mediated AMPK activation was not affected in the neonatal cardiomyocytes from MyD88$^{-/-}$ mice. The data represent three independent experiments. Values indicate densitometric ratio of pAMPK/AMPK or tubulin in immunoblots, mean ± SEM. Error bars indicate SEM. *P < 0.05 **P < 0.01 ***P < 0.001 compared with control.

showed that the AMPK activation started at 30 min, reached its peak at 60 min, and subsequently recovered (Fig. 1*D*), suggesting that the ATP decrease by TLR9 stimulation was a transient response. We further confirmed the decrease and time course of intracellular ATP levels in cardiomyocytes using a luminescence-based measurement (Fig. 1*E*). To extend our findings with CpG-ODN, we next tested if mitochondrial DNA could induce the unique TLR9 signaling in cardiomyocytes. Mitochondrial DNA (descended from bacterial DNA) is rich in unmethylated CpGs and is therefore a potent ligand for TLR9 (15). As cardiomyocytes possess abundant mitochondria (16), it is likely that higher amounts of this would be released in the heart during tissue damage than in other tissues. Indeed, mitochondrial DNA induced AMPK activation in cardiomyocytes in the same manner as synthetic CpG-ODN (Fig. S1*C*).

As the heart has low regenerative capacity, it is vital to protect as many surviving cardiomyocytes as possible from damaging inflammation. Therapeutic hypothermia has been shown to protect the heart and brain from injury by slowing metabolism and by switching on survival pathways (17). Also, well-known cardioprotective reagents including volatile anesthetics, nitric oxide, and beta blockers, reduce cardiac contractility, which is considered to be a part of the mechanism of cardioprotection (9). In addition, there are several lines of evidence showing that the activation of AMPK is cardioprotective (18, 19). Given our observation that TLR9 induced a negative inotropic effect with subsequent AMPK activation, we hypothesized that TLR9 exerts a protective effect in cardiomyocytes. Indeed, pretreatment with CpG-ODN significantly increased the cardiomyocyte survival against hypoxia compared with the vehicle control (Fig. 1*F*). An AMPK inhibitor (compound C) abrogated this protective effect of CpG-ODN (Fig. 1*F*), suggesting that AMPK is a mediator of the protective effect of TLR9.

Unique TLR9 Signaling in Cardiomyocytes Is Independent of Myeloid Differentiation Primary Response Gene 88 (MyD88). Next, to test whether the canonical inflammatory TLR9 signaling operates in cardiomyocytes, we compared the TLR9 response between RAW264.7 cells (a macrophage cell line) and cardiomyocytes. The inflammatory TLR9 response [i.e., IκBα degradation and phosphorylation (Fig. 1C and Fig. S2*A*), p38 MAPK phosphorylation (Fig. 1*C*), NF-κB [p65 subunit] nuclear translocation (Fig. S2 *B* and *C*), NF-κB electrophoretic mobility shift assay (Fig. S2*D*), NF-κB luciferase assay (Fig. S2*E*), and cytokine production (Fig. S2*F*)] was detected in RAW264.7 cells, but not in cardiomyocytes after CpG-ODN administration. In contrast, the phosphorylation of AMPK increased in cardiomyocytes, but not in RAW264.7 cells (Fig. 1*C*). These results suggest that the TLR9 signaling in cardiomyocytes is different from the canonical TLR9 signaling pathway in immune cells.

As the known inflammatory TLR9 signaling is mediated by a common TLR adaptor molecule, MyD88 (1), we next examined MyD88 involvement in the CpG-induced AMPK activation in cardiomyocytes by using MyD88$^{-/-}$ mice and MyD88 knockdown. The CpG-mediated AMPK activation was not affected in the neonatal cardiomyocytes by MyD88$^{-/-}$ mice (Fig. 1*G*) or by *Myd88* knockdown in rat cardiomyocytes (Fig. S1*D*). These data suggest that the alternative TLR9 signaling is MyD88 independent and branches from the canonical TLR9 signaling at the receptor level.

Unc93b1 Is a Pivotal Switch for the Distinct TLR9 Responses in Cardiomyocytes and Macrophages. To gain an insight into the mechanism by which the different TLR9 responses occur between cardiomyocytes and RAW264.7 macrophages, we performed RT-PCR screening for the known TLR9 signaling molecules. The results showed that *Unc93b1* was significantly less expressed in cardiomyocytes than in RAW264.7 cells (Fig. 2*A* and Fig. S2*A*).

Unc93b1 is the key molecule for TLR9 trafficking from the endoplasmic reticulum (ER) to the endosome/lysosomes and its cleavage (20). In macrophages and dendritic cells, the majority of TLR9 exists in the ER, whereas a minor fraction is present in the endosomes under resting condition (20, 21). After stimulation, TLR9 translocates to the endosome/lysosome compartment where MyD88 and the subsequent molecular complex initiate inflammatory signaling. Recently it was found that TLR9 ectodomain is cleaved in the endosome compartment, creating a C-terminal cleaved form (80 kDa) (22–25). Although both full-length (150

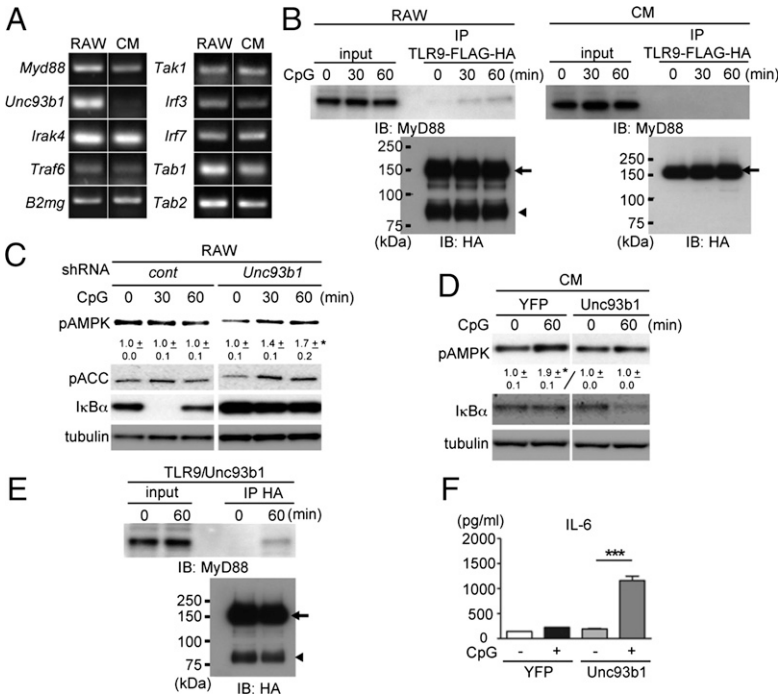

Fig. 2. *Unc93b1* is a pivotal switch for the distinct TLR9 responses in cardiomyocytes and immune cells. (*A*) RT-PCR screening of the TLR9 signaling molecules in RAW264.7 (RAW) and mouse neonatal cardiomyocytes (CM). *Unc93b1* was far less expressed in cardiomyocytes than in RAW264.7 cells. (*B*) MyD88 associated with TLR9 in RAW264.7 cells but not in cardiomyocytes. TLR9 was transiently transfected in both cardiomyocytes and RAW264.7 cells. The cell lysates were immunoprecipitated with anti-Flag antibody at 0, 30, or 60 min after CpG stimulation, immunoblotted with MyD88 antibody. A total of 1% of whole cell lysates was used as input. The molecular weight of overexpressed TLR9 in cardiomyocytes matched with the full-length form (arrow), but not to the cleaved form (arrowhead), whereas both forms were found in RAW264.7 cells. (*C*) The *Unc93b1* knockdown transformed the response to CpG-ODN in RAW264.7 cells from the inflammatory TLR9 signaling to the alternative TLR9 signaling that resulted in AMPK activation. The data represent three independent experiments. (*D–F*) Conversely, the overexpression of *Unc93b1* diminished TLR9-induced AMPK activation (*D*), switched on the inflammatory TLR9 signaling in cardiomyocytes with degradation of IκBα (*D*), appearance of the cleaved form of TLR9 (*E*), association with MyD88 (*E*), and subsequent inflammatory cytokine production (*F*). The cardiomyocytes, which were transfected with the indicated adenoviruses, were stimulated by CpG-ODN for 60 min (*D* and *E*) or 16 h ($n = 3$ for each group) (*F*). $^{***}P < 0.001$. Error bars indicate SEM. The data represent three independent experiments. Values indicate densitometric ratio of pAMPK/tubulin in immunoblots, mean ± SEM $^{*}P < 0.05$ compared with 0 min.

kDa) and cleaved forms can bind CpG DNA (22), only the cleaved form exists in endosomes (phagosome) and this cleavage is required/sufficient for recruiting MyD88 to its intracellular domain to initiate inflammatory signaling (25).

To test if the expression level of *Unc93b1* is a deciding factor for the different TLR9 responses, we first analyzed the molecular weight of TLR9 and its association with MyD88 in both cardiomyocytes and macrophages. The molecular weight of overexpressed TLR9 in cardiomyocytes was 150 kDa, which corresponds to the full-length form, and we could not detect the cleaved form of TLR9, whereas on the other hand both full-length and cleaved forms were observed in RAW264.7 cells (Fig. 2*B*, *Left*). The interaction between TLR9 and MyD88 was found in RAW264.7 cells, whereas in contrast, it was not detected in cardiomyocytes (Fig. 2*B*, *Right*). These results further confirmed that the alternative TLR9 signaling in cardiomyocytes is independent of MyD88.

We next tested whether RAW264.7 macrophages would behave similarly to cardiomyocytes when *Unc93b1* is inhibited. Of note, the knockdown of *Unc93b1* by shRNA reduced the inflammatory response upon CpG-ODN stimulation and instead AMPK activation occurred in RAW264.7 cells (Fig. 2*C* and Fig. S3 *B* and *C*). Conversely, the overexpression of *Unc93b1* in cardiomyocytes diminished TLR9-induced AMPK activation and instead switched on the inflammatory TLR9 signaling. *Unc93b1* overexpressing cardiomyocytes showed the cleaved form of TLR9, association between TLR9 and MyD88, degradation of IκBα, and subsequent cytokine production (Fig. 2 *D–F*), as seen in RAW264.7 cells.

Next we examined subcellular localization of TLR9 in cardiomyocytes. Unlike the translocation from the ER to endosome/lysosomes that has been reported in dendritic cells and macrophages (21), TLR9 stayed in the ER and did not translocate to the endosome compartment in cardiomyocytes before and after CpG-ODN stimulation (Fig. 3 *A* and *B*). In contrast, *Unc93b1* overexpression transformed the trafficking of TLR9 to early endsome antigen 1 (EEA1)-positive endosomes on CpG-ODN stimulation in cardiomyocytes (Fig. 3*C*), including an observation that a fraction of TLR9 localized in the endosome compartment before CpG-ODN stimulation (Fig. 3*C*), as previously reported in immune cells (20, 21).

Exogenous DNA Translocates to the ER to Bind TLR9 via Retrograde Transport in Cardiomyocytes. The results above raised a question of whether the endocytosed DNA really comes into contact with TLR9 in the ER to facilitate the alternative TLR9 signaling in cardiomyocytes, although it has been reported that DNA binds to the cleaved form of TLR9 in the endosome in immune cells (25). To answer this question, we investigated the localization of endocytosed DNA in cardiomyocytes using biotin-labeled CpG-ODN. Notably, it was found that CpG-ODN localized in the ER (Fig. 4*A*) 30 min after the administration of CpG-ODN. To exclude the possibility of detecting endogenous biotin, we confirmed the same pattern of localization by using FITC-labeled CpG-ODN (Fig. S4*B*, *Upper*), which was distinct from the punctate pattern of endocytosed DNA in RAW264.7 cells (Fig. S4 *A* and *B*), which is consistent with the previous report (21).

Exit from the endosomal compartment toward Golgi and ER is termed as retrograde transport and it has been reported that a number of proteins and lipids use this retrograde route to enter the Golgi and ER from endosome (26). Also retrograde transport is crucial to the cellular entry of certain pathogens or pathogenic products including toxins and viruses (26). Therefore, we speculated that translocation of endocytosed DNA used this retrograde transport route in cardiomyocytes. To elucidate this, we used Retro-2, an inhibitor for the retrograde transport without affecting endocytosis (27). Pretreatment with Retro-2 significantly changed the distribution pattern of CpG-ODN in cardiomyocytes (Fig. 4*B*). The speckled accumulation of endocytosed CpG-ODN was overlapped with EEA1-positive endosomes, indicating that cardiomyocytes indeed use the retrograde transport for exogenous DNA. To support this, Retro-2 indeed reduced the TLR9-mediated AMPK activation in cardiomyocytes (Fig. 4*C*). Interestingly, Retro-2 also inhibited the CpG-ODN–induced AMPK activation in the *Unc93b1* knocked-down RAW264.7 cells (Fig. 4*D*). Although the distribution of biotin-labeled CpG-ODN (green) in control RAW264.7 cells was a punctate pattern, it became spread and less punctate in *Unc93b1* knocked-down RAW264.7 cells (Fig. S5 *A* and *B*). These data suggest that expression level of *Unc93b1* affects the trafficking of endocytosed DNA and TLR9. We speculate that preexistence of TLR9 at the endosome and following supply from the ER after stimulation (20, 21, 28) (in control RAW or *Unc93b1*-overexpressing cardiomyocytes shown in Fig. 3*C*) enables

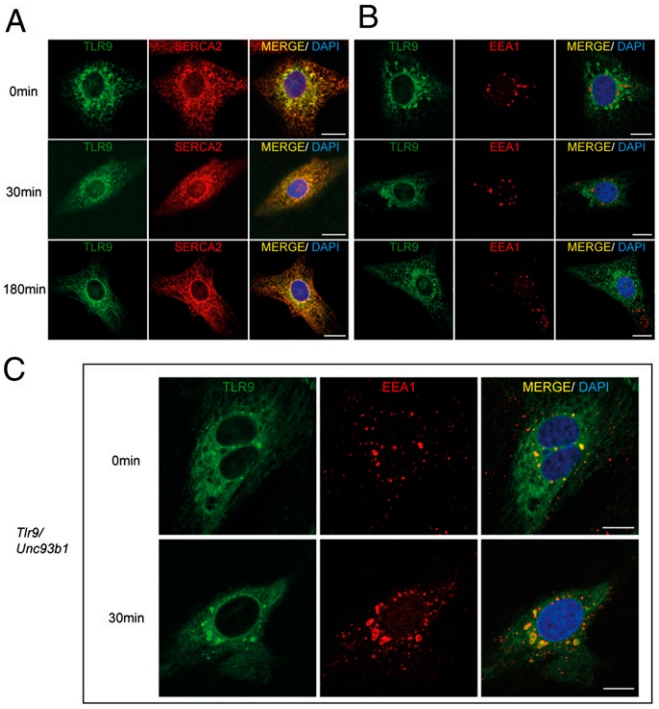

Fig. 3. *Unc93b1* overexpression transformed the trafficking of TLR9 in cardiomyocytes. (*A*) TLR9 (HA; green) stayed in the ER [sarcoplasmic/endoplsmic reticulum Ca^{2+}-ATPase (SERCA2); red] at any time points of 0, 30, and 180 min after CpG-ODN stimulation in cardiomyocytes. (*B*) TLR9 did not translocate to the endosome compartment (EEA1; red) in cardiomyocytes regardless of before and after CpG-ODN stimulation. (*C*) *Unc93b1* overexpression transformed the trafficking of TLR9 to EEA1-positive endosomes in cardiomyocytes. Please note that part of TLR9 existed in the endosome compartment before stimulation. The cardiomyocytes, which were transfected with the adenoviruses encoding TLR9-HA-Flag (*A*–*C*) and Unc93b1 in (*C*), were stimulated by CpG-ODN. (Scale bars, 10 μm.) Images were obtained with confocal microscopy. Experiments were repeated at least twice and the representative images are shown.

the majority of endocytosed DNA to be trapped by TLR9 at the endosome, resulting in the initiation of the canonical inflammatory signaling. In contrast, very little existence of TLR9 at the endosome and little supply from the ER after stimulation due to low level of *Unc93b1* expression will allow DNA to travel to the ER via the retrograde transport system, exerting the alternative TLR9 signaling (Fig. 5*E*). Collectively, we conclude that exogenous DNA translocates to the ER via the retrograde transport to bind TLR9 in cardiomyocytes.

Alternative TLR9 Signaling also Operates in Differentiated Neuronal Cells. We further investigated whether the alternative TLR9 signaling found in cardiomyocytes is applicable to other nonimmune cells more generally. To examine this, we used human SH-SY5Y cells, which after sequential treatment with retinoic acid and BDNF yield terminally differentiated neuronal cells (29). Although undifferentiated SH-SY5Y cells showed only a subtle increase in phosphorylated AMPK after CpG-ODN stimulation, the differentiated neuronal cells demonstrated a robust and transient increase in phosphorylated AMPK without any degradation of IκBα (Fig. 5*A*). CpG-ODN stimulation significantly decreased intracellular ATP levels in the differentiated neuronal cells (Fig. 5*B*). We also found the endocytosed CpG-ODN localized in the ER (Fig. S4). These data suggest that the same alternative TLR9 signaling we observed in cardiomyocytes also operates in neuronal cells. Compared with human monocytes/macrophages, the expression level of *Unc93b1* remained low in SH-SY5Y cells regardless of the differentiation status, whereas *Tlr9* expression significantly increased in the differentiated neuronal status (Fig. 5*C*), which might account for the different extent of the unique TLR9 responses between two differentiation states. Finally, the pretreatment with CpG-ODN decreased cell death and increased cell viability after hydrogen peroxide insult in the differentiated neuronal cells (Fig. 5*D*).

Discussion

In this study, we revealed an unexpected role of TLR9 in energy metabolism and cellular protection in not only cardiomyocytes but also in neuronal cells. Importantly, the alternative TLR9 signaling in these cells is independent of the canonical inflammatory signaling in immune cells, although the two pathways are interchangeable by the expression level of *Unc93b1*.

On the basis of these findings, we propose an intriguing model of biological adaptation, in which nonimmune cells with low expression level of *Unc93b1* will sense the danger signal from damaged cells upon injury, reduce energy consumption, and consequently increase the stress tolerance through AMPK activation, whereas immune cells with higher expression of *Unc93b1* initiate an inflammatory response (Fig. 5*E*). The concept that the same ligand–receptor in innate immunity can concomitantly increase the stress tolerance in cardiomyocytes and neurons, whereas immune cells induce inflammation upon tissue injury, will shed alternative light on our understanding of innate immunity.

One important finding in our study is that Unc93b1 is the pivotal switch for the distinct TLR9 responses. Also we found that the alternative TLR9 is independent of MyD88. Thus, a strategy to dissect innate immune responses between immune and nonimmune cells will synergistically induce a protective effect against tissue injury: enhancing the self-protective TLR9 signaling in cardiomyocytes and neurons, concurrently with the systemic inhibition of Unc93b1 or MyD88, which could achieve effective attenuation of damaging inflammation, may have clinical implication.

Furthermore, our study may have an implication in chronic inflammation, which is a major pathogenesis/modulator for a wide range of diseases, such as heart failure, neurodegenerative diseases, and metabolic syndrome. Dysregulation of the response to endogenous ligands is known to be important for sustaining chronic inflammation in metabolic syndrome (30). Our data showed that the expression level of *Unc93b1* is the deciding factor for the distinct TLR9 signaling pathways; hence, altered expression of *Unc93b1* can transform TLR9 signaling from protective to inflammatory in nonimmune cells in pathological conditions.

Recently Oka et al. reported mitochondrial DNA that escapes from degradation in the lysosome can trigger an inflammatory response in cardiomyocytes in pressure-overloaded heart (31). Discrepancy in our observation and theirs may be caused by the different status of cardiomyocytes; healthy or under the pathologic condition of pressure overload. Pressure overload heavily induces oxidative stress in cardiomyocytes and alters the gene expression profile with significant epigenetic modulation (32–34). It may lead to altered *Unc93b1* expression, enabling cardiomyocytes to induce canonical inflammatory signaling in response to mitochondrial DNA, as we observed in *Unc93b1* overexpressing cardiomyocytes. Another possibility is the difference in transport route for DNA, as mitochondrial DNA escaping autophagy is not released into the extracellular space according to their report, unlike our model using exogenous DNA; although our finding that endocytosed DNA reached the ER via retrograde transport system was based on the experiment using a single inhibitor. Further study, e.g., specific knockdown of members of the retromer complex, would be required to conclusively demonstrate this transport route. Nevertheless, future investigation of the TLR9 signaling in cardiomyocytes under pathological conditions is warranted and may provide better understanding of these diseases and alternative therapeutic options.

In this manuscript, we found the alternative TLR9 signaling that reduces energy substrates to protect cardiomyocytes and neurons by activating AMPK. There are two possibilities for the decrease in energy substrates (intracellular ATP levels): either an

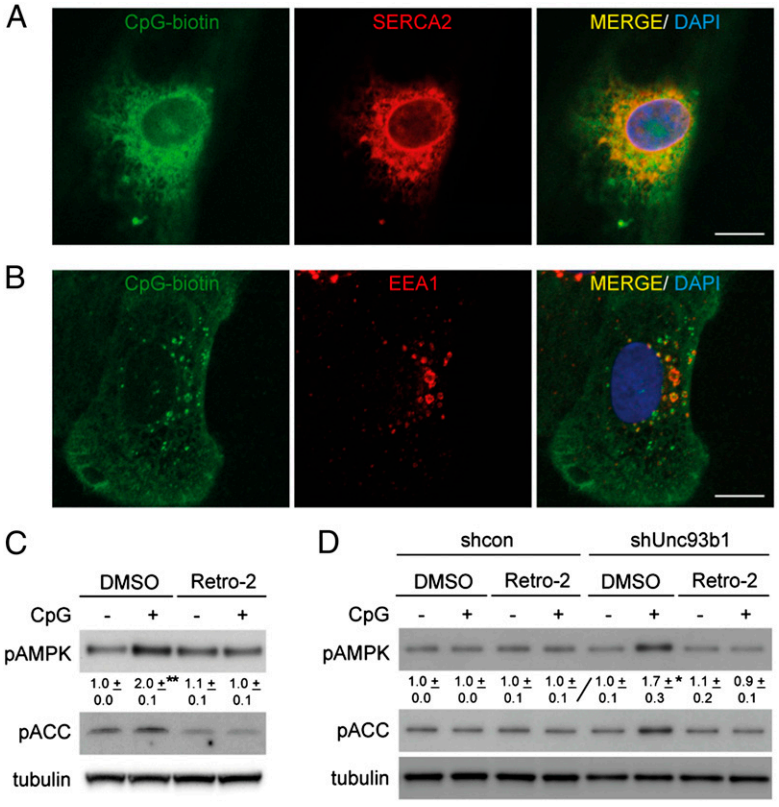

Fig. 4. Endocytosed DNA translocates to the ER via retrograde transport system in cardiomyocytes. (*A*) Biotin-labeled CpG-ODN (green) localized in the ER (SERCA2; red) 30 min after administration in cardiomyocytes. (*B*) Retro-2 (100 μM for 30 min pretreatment before administration of CpG-ODN), the inhibitor or retrograde transport, changed the distribution pattern of endocytosed DNA in cardiomyocytes. Endocytosed CpG-ODN accumulated in EEA1-positive endosomes (red). (Scale bars, 10 μm.) Images were obtained with confocal microscopy. Experiments were repeated at least twice and the representative images are shown. (*C*) Retro-2 inhibited the TLR9-mediated AMPK activation in cardiomyocytes. The data represent four independent experiments. (*D*) Retro-2 also inhibited the CpG-ODN–induced AMPK activation in the *Unc93b1* knocked-down RAW264.7 cells, but not in control RAW cells. The data represent four independent experiments. Values indicate densitometric ratio of pAMPK/tubulin in immunoblots, mean ± SEM $*P < 0.05$, $**P < 0.01$ compared with the control.

increase in energy expenditure or a decrease in ATP synthesis. Considering that we observed decreased contraction throughout the ex vivo heart experiment, it is unlikely to be caused by increased energy expenditure, rather a decrease in ATP synthesis

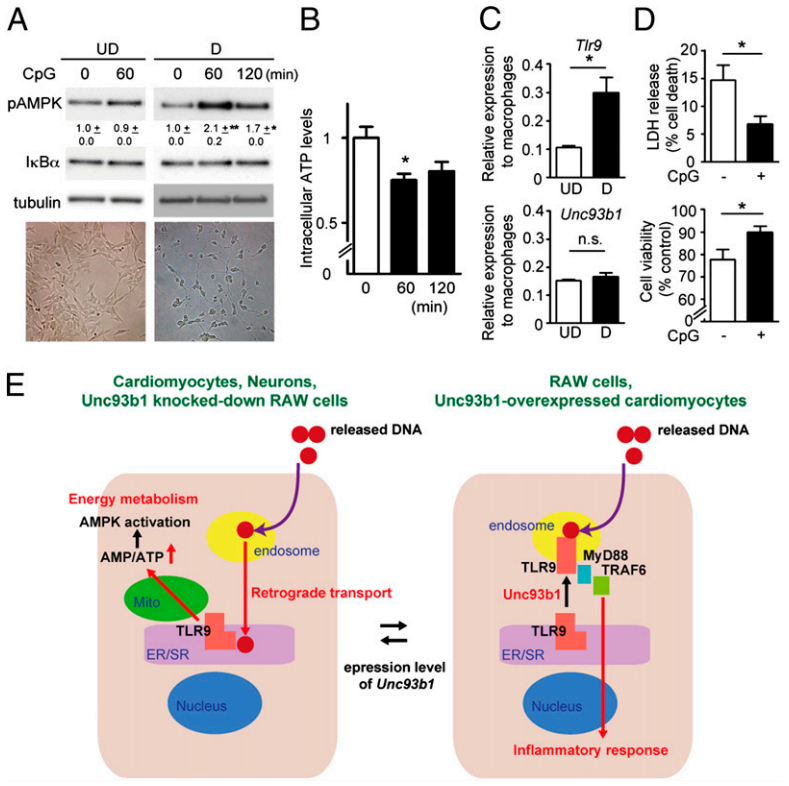

Fig. 5. The alternative protective TLR9 signaling also operates in differentiated neuronal cells. (*A*) Differentiated neuronal cells (*Right*; D) demonstrated a robust and transient increase in phosphorylated AMPK after CpG-ODN stimulation without degradation of IκBα, whereas undifferentiated SH-SY5Y cells (*Left*, UD) showed a subtle increase in phosphorylated AMPK. Typical morphology of the corresponding differentiation status is shown below the blots. The data represent three independent experiments. Values indicate densitometric ratio of pAMPK/tubulin in immunoblots, mean ± SEM $*P < 0.05$, $**P < 0.01$ compared with 0 min. (*B*) Administration of CpG-ODN significantly reduced intracellular ATP levels in the differentiated neuronal cells 60 min after treatment. $n = 3$ for each group. The data represent two independent experiments. (*C*) *Tlr9* expression significantly increased along with the differentiation status (*Upper*), whereas the expression level of *Unc93b1* remained low regardless of differentiation (*Lower*). The expression level was normalized to the level of human monocytes/macrophages, U937 cells which were differentiated with 10 nM phorbol 12-miristate 13-acetate (PMA) ($n = 4$–5 for each group). $*P <$ 0.05 compared with the undifferentiated SH-SY5Y cells. (*D*) Pretreatment with CpG-ODN significantly decreased cell death (assessed by lactate dehydrogenase release; *Left*) and increased cell viability (measured by MTT assay; *Right*) after hydrogen peroxide (25 μM for 24 h, $n = 12$ for each group) in differentiated neuronal cells. $*P < 0.05$ compared with the control. $*P < 0.05$. Error bars indicate SEM. (*E*) Schematic presentation of two different TLR9 signaling pathways. Cardiomyocytes or neurons with low expression level of *Unc93b1* sense released DNA (danger signal) at the ER from damaged cells upon injury, reduce energy metabolism, and consequently increase the stress tolerance through AMPK activation, whereas immune cells with higher expression of *Unc93b1* initiate the inflammatory response at the endosome. The alternative and inflammatory TLR9 signaling pathways are interchangeable depending on the expression levels of *Unc93b1*.

would be a more probable explanation. A brief episode of reversible ischemia before the prolonged ischemia induces powerful tissue protection, referred to as ischemic preconditioning (IPC) (35). Interestingly, IPC reduces mitochondrial ATP synthesis during IPC; however, it prevents further decrease in intracellular ATP after sustained ischemia (9). Also it has been known that a number of drugs, which reversibly inhibit mitochondrial metabolism, improve recovery from ischemia reperfusion injury (9). It is an intriguing concept that an endogenous molecule, DNA, released from damaged cells upon tissue injury, induces energy starvation to switch on cellular protective machinery in non-immune cells, e.g., cardiomyocytes and neurons. Further research into the mechanism by which TLR9 in the ER reduces intracellular ATP levels will be of interest and currently is under investigation in our laboratory.

Materials and Methods

Mice and Reagents. TLR9$^{-/-}$ and MyD88$^{-/-}$ mice were generated in Shizuo Akira's laboratory (Osaka University, Osaka) and purchased from Oriental Kobo with C57BL6 background (Kyoto). C57BL6 wild-type mice were obtained from Charles River. CpG-ODN 2216 (CpG type A), CpG-ODN 1668 (CpG type B), FITC-labeled CpG-ODN 1668, biotin-labeled CpG-ODN 1826 (CpG type B), TLR2 ligand (HKLM), TLR4 ligand (LPS-EB Ultrapure) and TLR7 ligand (imiquimod) were purchased from Source BioScience. Compound C and Retro-2 were purchased from Merck. Oligomycin A was purchased from Sigma. ER tracker red was purchased from Invitrogen.

Antibodies. Antibodies for SERCA2 (Abcam; ab3625), phopsho-AMPK (Cell Signaling; 2535), AMPK (Cell Signaling; 2532), phospho-ACC (Cell Signaling; 3661), ACC (Cell Signaling; 3676), phospho-IκBα (Cell Signaling; 9246), IκBα (Cell Signaling; 9242), NF-κB (p65) (Cell Signaling; 4764), EEA-1 (Cell Signaling; 2411), tubulin (Sigma; B-5-1-2), HA (Roche; 3F10), phospho-p38MAPK (Cell Signaling; 9216), and MyD88 (Abcam; ab2064) were purchased as presented. Anti-Flag (M2) affinity matrices were purchased from Sigma.

Cell Culture. Primary cultures of neonatal rat cardiomyocytes were prepared from 2- to 3-d-old Wistar rats. Harvested hearts were incubated in 0.25% trypsin/EDTA (Sigma) at 4 °C overnight and then digested with collagenase type II (Worthington). The cardiomyocyte fraction was collected after differential plating for 70 min at 37 °C, counted, and seeded onto gelatin-coated dishes or fibronectin-coated glass-bottom dishes. For mouse neonatal cardiomyocytes, 0.05% trypsin/EDTA was used. Cardiomyocytes were cultured in DMEM (Sigma) supplemented with 5% (wt/vol) FBS. One day after isolation, cardiomyocytes were treated with mitomycin C (10 μg/mL; Sigma) for 2 h to inhibit growth of other cell types contaminating the culture. Cells were normally used for experiments 4–6 d after isolation. The medium was changed to DMEM containing 2% FBS for 30 min before CpG-ODN administration. For Ca^{2+} transient and mitochondrial Ca^{2+} experiments, media were supplemented with 3.6 mM Ca^{2+}. RAW264.7 cells were obtained from European Collection of Cell Culture (ECACC) and maintained in DMEM supplemented with 10% FBS. The SH-SY5Y human neuroblastoma cells were obtained from ATCC and maintained in DMEM/F12 supplemented with 10% FBS. For differentiation, cells were seeded at an initial density of 10^4 cells/cm^2 in culture dishes. All-transretinoic acid (RA) (Sigma) was added the day after plating at a final concentration of 10 μM in DMEM/F12 with 3% FBS. After 5 d in the presence of RA, the cells were washed with DMEM/F12 and incubated with 50 ng/mL BDNF (Peprotech) in DMEM/F12 without serum for 3 d (29). Before experiments, the medium was replaced with neurobasal medium (Invitrogen) with B27 supplement (Invitrogen). U937 cells were obtained from ECACC and maintained in RPMI supplemented with 10% FBS. For differentiation to the macrophage phenotype, the cells were treated with 10 nM PMA for 16 h, then incubated with RPMI supplemented with 10% FBS for 3 d.

Further methods and additional discussion are found in *SI Discussion 1*, *SI Discussion 2*, and *SI Materials and Methods*.

ACKNOWLEDGMENTS. We thank Melanie M. Brinkmann for the mTLR9-myc construct; Paul Chapple for SH-SY5Y cells; Hannes C. A. Drexler, Cesare M. N. Terracciano, Hiromi Imamura, Hidetaka Kioka, Shizuo Akira, Osamu Takeuchi, Kinya Otsu, and Masaharu Akao for help and suggestions on this project; and members of the K.S. laboratory. This research was supported by the New Investigator Research Grant from the Medical Research Council (G1000461 to Y.S.), the Barts and the London Charity, and the National Institute for Health Research Cardiovascular Biomedical Research Unit. Y.S. is also supported by the Uehara Memorial Foundation.

1. Kawai T, Akira S (2010) The role of pattern-recognition receptors in innate immunity: Update on Toll-like receptors. *Nat Immunol* 11(5):373–384.
2. Arumugam TV, et al. (2009) Toll-like receptors in ischemia-reperfusion injury. *Shock* 32(1):4–16.
3. Kono H, Rock KL (2008) How dying cells alert the immune system to danger. *Nat Rev Immunol* 8(4):279–289.
4. Hemmi H, et al. (2000) A Toll-like receptor recognizes bacterial DNA. *Nature* 408 (6813):740–745.
5. Haas T, et al. (2008) The DNA sugar backbone 2′ deoxyribose determines toll-like receptor 9 activation. *Immunity* 28(3):315–323.
6. Crack PJ, Bray PJ (2007) Toll-like receptors in the brain and their potential roles in neuropathology. *Immunol Cell Biol* 85(6):476–480.
7. Boyd JH, Mathur S, Wang Y, Bateman RM, Walley KR (2006) Toll-like receptor stimulation in cardiomyoctes decreases contractility and initiates an NF-kappaB dependent inflammatory response. *Cardiovasc Res* 72(3):384–393.
8. Paladugu B, et al. (2004) Bacterial DNA and RNA induce rat cardiac myocyte contraction depression in vitro. *Shock* 21(4):364–369.
9. Burwell LS, Nadtochiy SM, Brookes PS (2009) Cardioprotection by metabolic shutdown and gradual wake-up. *J Mol Cell Cardiol* 46(6):804–810.
10. Kahn BB, Alquier T, Carling D, Hardie DG (2005) AMP-activated protein kinase: ancient energy gauge provides clues to modern understanding of metabolism. *Cell Metab* 1(1):15–25.
11. Carling D (2004) The AMP-activated protein kinase cascade—a unifying system for energy control. *Trends Biochem Sci* 29(1):18–24.
12. Hardie DG (2003) Minireview: The AMP-activated protein kinase cascade: the key sensor of cellular energy status. *Endocrinology* 144(12):5179–5183.
13. Terai K, et al. (2005) AMP-activated protein kinase protects cardiomyocytes against hypoxic injury through attenuation of endoplasmic reticulum stress. *Mol Cell Biol* 25(21):9554–9575.
14. Jeon S-M, Chandel NS, Hay N (2012) AMPK regulates NADPH homeostasis to promote tumour cell survival during energy stress. *Nature* 485(7400):661–665.
15. Zhang Q, et al. (2010) Circulating mitochondrial DAMPs cause inflammatory responses to injury. *Nature* 464(7285):104–107.
16. Hattori F, et al. (2010) Nongenetic method for purifying stem cell-derived cardiomyocytes. *Nat Methods* 7(1):61–66.
17. Polderman KH (2009) Mechanisms of action, physiological effects, and complications of hypothermia. *Crit Care Med* 37(7, Suppl):S186–S202.
18. Russell RR, 3rd, et al. (2004) AMP-activated protein kinase mediates ischemic glucose uptake and prevents postischemic cardiac dysfunction, apoptosis, and injury. *J Clin Invest* 114(4):495–503.
19. Miller EJ, et al. (2008) Macrophage migration inhibitory factor stimulates AMP-activated protein kinase in the ischaemic heart. *Nature* 451(7178):578–582.
20. Kim Y-M, Brinkmann MM, Paquet M-E, Ploegh HL (2008) UNC93B1 delivers nucleotide-sensing toll-like receptors to endolysosomes. *Nature* 452(7184):234–238.
21. Latz E, et al. (2004) TLR9 signals after translocating from the ER to CpG DNA in the lysosome. *Nat Immunol* 5(2):190–198.
22. Ewald SE, et al. (2008) The ectodomain of Toll-like receptor 9 is cleaved to generate a functional receptor. *Nature* 456(7222):658–662.
23. Park B, et al. (2008) Proteolytic cleavage in an endolysosomal compartment is required for activation of Toll-like receptor 9. *Nat Immunol* 9(12):1407–1414.
24. Sepulveda FE, et al. (2009) Critical role for asparagine endopeptidase in endocytic Toll-like receptor signaling in dendritic cells. *Immunity* 31(5):737–748.
25. Ewald SE, Barton GM (2011) Nucleic acid sensing Toll-like receptors in autoimmunity. *Curr Opin Immunol* 23(1):3–9.
26. Johannes L, Popoff V (2008) Tracing the retrograde route in protein trafficking. *Cell* 135(7):1175–1187.
27. Stechmann B, et al. (2010) Inhibition of retrograde transport protects mice from lethal ricin challenge. *Cell* 141(2):231–242.
28. Brinkmann MM, et al. (2007) The interaction between the ER membrane protein UNC93B and TLR3, 7, and 9 is crucial for TLR signaling. *J Cell Biol* 177(2):265–275.
29. Encinas M, et al. (2000) Sequential treatment of SH-SY5Y cells with retinoic acid and brain-derived neurotrophic factor gives rise to fully differentiated, neurotrophic factor-dependent, human neuron-like cells. *J Neurochem* 75(3):991–1003.
30. Fessler MB, Rudel LL, Brown JM (2009) Toll-like receptor signaling links dietary fatty acids to the metabolic syndrome. *Curr Opin Lipidol* 20(5):379–385.
31. Oka T, et al. (2012) Mitochondrial DNA that escapes from autophagy causes inflammation and heart failure. *Nature* 485(7397):251–255.
32. Nabeebaccus A, Zhang M, Shah AM (2011) NADPH oxidases and cardiac remodelling. *Heart Fail Rev* 16(1):5–12.
33. Heineke J, Molkentin JD (2006) Regulation of cardiac hypertrophy by intracellular signalling pathways. *Nat Rev Mol Cell Biol* 7(8):589–600.
34. Zhang CL, et al. (2002) Class II histone deacetylases act as signal-responsive repressors of cardiac hypertrophy. *Cell* 110(4):479–488.
35. Jennings RB, Murry CE, Reimer KA (1991) Preconditioning myocardium with ischemia. *Cardiovasc Drugs Ther* 5(5):933–938.

Supporting Information

Shintani et al. 10.1073/pnas.1219243110

SI Discussion 1

Recently, Knuefermann et al. reported that Toll-like receptor 9 (TLR9)-mediated NF-κB nitric oxide synthase 2 (NOS2) induction and negative inotropic effect were observed 4 h, but not in the first 1–3 h, after administration of CpG-oligodeoxynucleotides (CpG-ODN) in isolated mouse adult cardiomyocytes (1). In contrast, we used neonatal cardiomyocytes from rat and mouse (Fig. 1 *C*, *D*, and *G*) and did not observe any NF-κB activation at earlier time points (30–60 min) and up until 3 h.

The major difference between our findings and their findings is the time course analyzed. This can be well explained by the class II characteristics of NOS2 induction after TLR stimulation (2). The previous extensive research demonstrated that, even though NF-κB activation occurs at early time points, TLRs (NF-κB) target genes are classified into three groups; primary response genes (class I), secondary response genes (class II), and tertiary response genes (class III) (2). NOS2 is one of the most extensively studied target genes and well classified as a class II gene, which are up-regulated 2–8 h after stimulation because they require de novo protein synthesis of cofactors including the class I genes (3). Therefore, it is unlikely that rapid NOS2 induction occurs within the time frame of 30–60 min after stimulation.

In relevance to this issue, to exclude the possibility of NO induction via activation of any NOS member without transcription in cardiomyocytes at the time point we focused on, we tested the effect of nonspecific NOS inhibitor, N(G)-nitro-L-arginine methyl ester (L-NAME), and confirmed that there was no NO involvement in TLR9-mediated AMPK activation (Fig. S7*B*).

Therefore, we conclude that the alternative TLR9 signaling we report here is NF-κB–NO independent, not from the canonical mechanism of TLR9 signaling.

SI Discussion 2

To answer whether our findings are specific to TLR9 or not, we checked the response to stimulation of TLR2, -4 (cell surface TLRs), and also TLR7 (nucleotide sensing, an ER endosome). Whereas there was no AMPK activation after TLR2 or -4 stimulation, TLR7 stimulation significantly increased AMPK phosphorylation. (Fig. S7*A*). According to the previous literature reporting that unc93 homolog B1 (*C. elegans*) (Unc93b1) interacts with intracellular TLRs (TLR3, -7, and -9) (4, 5), but not with plasma membrane TLRs, it is likely that the similar mechanism to TLR9 is applied to other intracellular, nucleotide-sensing TLRs.

SI Materials and Methods

Plasmids and Viral Vector Construction. Mouse TLR9-myc cDNA was a kind gift from Melanie Brinkmann (Whitehead institute for Biomedical Research, Cambridge, MA). C-terminal myc was replaced with HA-Flag tag by a PCR-based method. The amplified fragment was inserted to pENTR1A (Invitrogen) and the sequence was verified. Human *Unc93b1* cDNA was purchased from Open Biosystems and cloned into pENTR1A. The subcloned cDNA was transferred to pAd/CMV/V5-DEST (Invitrogen) using the Gateway system (Invitrogen). Adenovirus was generated using ViraPower Adenoviral Expression system (Invitrogen) as described by the manufacturer, following purification using Vivapure AdenoPACK (Satorius Stedim Biotech). TLR9-HA-Flag was subcloned to pWPXL (Addgene) by normal restriction enzymatic method, and then lentiviral particles were generated in 293T cells by calcium-phosphate precipitation transfection with pCMVdelta8.2 and pMD2.G.

RNAi. To knockdown *Unc93b1*, lentiviral particles derived from the pLKO.1-puro–containing the shRNA sequence (TRCN0000173466) were purchased from the Mission shRNA library (Sigma). The shControl was purchased from Sigma. RAW264.7 cells were infected with the lentiviral particles in the presence of 8 μg/mL polybrene. Puromycin (5 μg/mL; Invitrogen) was used for selection. To knock down *Myd88*, cardiomyocytes were transfected with siRNAs (5 nM) using lipofectamine RNAi MAX (Invitrogen) 4–6 h after isolation; MyD88-1 (sense: gaggagagcuauuugauuaTT; antisense: uaaucaaauagcucuccucTT), MyD88-2 (sense: gcuguuugguguagguaaaTT; antisense: uuuaccuacaccaaacagcTT) (Ambion). As a negative control, siControl (Ambion) was used.

Langendorff Perfusion. Mice were anesthetized with ketamine (100 mg/mL) and xylazine (20 mg/mL) mixture [2:1; 1.5 μL/g of body weight (BW), intraperitoneally) and heparinized (heparin sodium, 1 IU/g of BW, intraperitoneally). Following a thoractomy, the heart was excised and rapidly transferred to ice-cold Krebs–Henseleit buffer (KHB), containing (in millimoles) NaCl 118, KCL 3.8, $MgSO_4$ 1.19, $NaHCO_3$ 25, $CaCl_2$ 1.25, KH_2PO_4 1.18, sodium pyruvate 5, and glucose 10; equilibrated with 95% O2/5% CO_2 (pH 7.4). Aortic cannulation was performed (within 1 min of excision), and hearts were perfused with filtered KHB gassed continuously with 95% O2/5% CO_2 and maintained at 37 °C. Hearts were retrogradely perfused in a recirculating Langendorff mode. Coronary flow was monitored and adjusted using a flow meter to achieve a coronary perfusion pressure of 75 ± 5 mmHg. Hearts were allowed to stabilize for at least 15 min before any experimental protocols were carried out. A handmade balloon connected to a polyethylene tube was inserted into the left ventricle (LV) through the mitral valve via an incision in the left atrium and was connected to a pressure transducer (AD Instruments). Recorded waveforms were analyzed using chart 5 (AD Instruments) and maximal rate of pressure rise (LV dP/dt max) were calculated from the average of at least 50 cardiac cycles. LV dP/dt max is a reasonable index of the contractile ability of the heart.

Hypoxia and Cell Viability Assay. Hypoxia (<1% oxygen for 16 h) was achieved using a hypoxic chamber (Beckton Dickinson), which caused 52% cardiomyocyte death. Cell viability was assessed with MTT assay. Briefly, after hypoxia or H_2O_2, the medium was changed to medium containing MTT (0.4 mg/mL) and incubated for 60 min at 37 °C. After removal of the MTT medium, DMSO was added, and solubilized formazan was measured at 550 nm with a microplate reader. The cells with normoxia throughout the experiment or without H_2O_2 were regarded as 100% viable.

Cytotoxicity Assay. The differentiated neuronal cells in a 24-well format with neurobasal medium including B27 supplement were pretreated with or without CpG-ODN (type B; 3 μM for 30 min), then incubated with H_2O_2 (25 μM) for 24 h. Collected supernatants were subjected to lactate dehydrogenase assay (Sigma). Cells without H_2O_2 were lysed with 1% Triton X-100, regarded as 100% cells dead.

Confocal Microscopy. Cardiomyocytes or RAW264.7 cells were plated onto laminin or fibronectin-coated eight-well chamber slides (Nunc) or glass-bottom dishes (Iwaki). Cells were then stimulated with or without CpG-ODN, washed with PBS, and fixed with 4% paraformaldehyde at room temperature for 10 min. After washing with PBS, cells were permeabilized with 0.1% Triton X-100 and blocked with 5% goat serum or 1% BSA. Primary antibodies were then applied and incubated at 4 °C overnight. After labeling with

Alexa 488- or 555-conjugated secondary antibody or streptavidin (Invitrogen), images were obtained using LSM 710 confocal microscopy (Zeiss) with 1 μm thickness using 63× objective lens. At least 20 cells were examined per condition and representative images were chosen.

Measurements of Energy Substrates in the Heart Using High Performance Liquid Chromatography. All measurements of metabolite concentrations were performed using high performance liquid chromatography (HPLC) as described previously (6). The AMP/ATP ratio was calculated from phosphocreatine, creatine, and ATP concentrations as described earlier assuming constant pH and Mg^{2+} concentration (7).

Intracellular ATP Measurement. Intracellular ATP levels were measured using ATP Bioluminescence Assay kit HS II (Roche), according to the manufacturer's instructions. Values were normalized by the average of the control cells.

Mitochondrial DNA Extraction and Purity Check. Mitochondrial DNA was isolated from female Wistar rat hearts using a mitochondria isolation kit (Thermo Scientific), according to the manufacturer's instructions, followed by the DNeasy kit (Qiagen). Extracted DNA was tested for its purity by PCR using genomic (*Tlr9* locus, 5′-ctagacgtgagaagcaaccctctg and 5′-cagctcgttatacacccagtcggc) or mitochondrial (*CytB*; 5′-gcattttcatcagtcaccca and 5′-gagtttaatcctgtggggtt) primer sets.

ELISA and Western Blotting. For ELISA, cells were treated with CpG-ODN (type B; 3 μM) for 16 h. For cardiomyocytes, 24 h after transfection of YFP or Unc93b1 in addition to TLR9-HA-Flag adenoviruses, cells were treated with CpG-ODN. The collected supernatant was analyzed using rat or mouse IL-6 and TNF-α–specific ELISA kits (R&D and eBioscience). For Western blotting, cells were washed with PBS and directly lysed with SDS/PAGE sample buffer to inhibit phosphatases and proteinases during cell lysis.

Semiquantitative RT-PCR and Real-Time PCR. Total RNA was prepared using RNeasy kits (Qiagen) with DNase I treatment and converted to cDNA with random primers using High Capacity cDNA Reverse Transcription kits (Applied Biosystems) according to the manufacturer's instructions. After optimization of at least three different PCR cycles, the amplified samples in electrophoresis were assessed by densitometry. Real-time PCR was performed using SYBR green with RG-6000 (Corbett) and comparative quantitation was made as previously described (8). All samples were measured in duplicate. The level of each expression was normalized with beta-2 microglobulin (*β2m*) (semiquantitative) ubiquitin C (*Ubc*) (real-time PCR) as housekeeping genes. The primers used in this study are shown in Fig. S8.

Nuclear/Cytosolic Fraction and NF-κB Electrophoretic Mobility Shift Assay. NF-κB electrophoretic mobility shift assay was performed as previously described (9).

Nuclear extracts were harvested from 5×10^6 cells. Briefly, cells were washed in ice-cold PBS and resuspended in 200 μL of buffer A (10 mM Hepes, pH 7.9, 10 mM KCl, 0.1 mM EDTA, 1 mM DTT plus a mixture of protease inhibitors). After 10 min on ice, cells were lysed by addition of Nonidet P-40 in a final concentration of 0.1%, and lysates were spun down for 1 min. Cell pellets were washed with 200 μL of buffer A and then resuspended in 50 μL of buffer B (20 mM Hepes, pH 7.9, 400 mM NaCl, 1 mM EDTA, 1 mM DTT plus a mixture of protease inhibitors) for 60 min. The supernatants containing the nuclear fractions was then collected by centrifugation for 5 min at $13{,}000 \times g$, then subjected to further analysis. The nuclear extract (7.5 μg) from cardiomyocytes or RAW264.7 cells was incubated with ^{32}P end-labeled, double-stranded oligonucleotide probes in the binding buffer [10 mM Tris·HCl (pH 7.5), 50 mM NaCl, 1 mM EDTA, 3 mM GTP, 5% glycerol, 1 mg/mL albumin, 0.1 mg/mL poly (dI:dC) and 1 mM DTT], and fractionated in a 4% polyacrylamide gel. The NF-κB double-stranded oligonucleotide probe was purchased from Promega.

NF-κB Luciferase Assay. NF-κB luciferase assay was performed as previously described (10). Briefly, neonatal cardiomyocytes and RAW264.7 cells were transfected with NF-κB–luciferase reporter plasmid and Renilla luciferase plasmid for transfection control by using electroporation (Amaxa; Nucleofector) according to the manufacturer's instructions. Using GFP-expressing construct, we confirmed ∼40% of cardiomyocytes were transfected with this method. Cells were treated for 3 h with the CpG-ODN. After cell lysis, NF-κB stimulation was measured through luciferase activity. Relative light units were calculated in reference to luciferase activity of medium alone.

Statistical Analysis. The comparison between two groups was made by *t* test (two tailed), and other comparisons were made by ANOVA followed by Bonferroni's post hoc test. Time-lapse data were assessed by two-way ANOVA repeated measure followed by Bonferroni's post hoc. A value of $P < 0.05$ was considered statistically significant. Error bars indicate SEM.

1. Knuefermann P, et al. (2008) Bacterial DNA induces myocardial inflammation and reduces cardiomyocyte contractility: Role of toll-like receptor 9. *Cardiovasc Res* 78(1): 26–35.
2. Medzhitov R, Horng T (2009) Transcriptional control of the inflammatory response. *Nat Rev Immunol* 9(10):692–703.
3. Buxadé M, et al. (2012) Gene expression induced by Toll-like receptors in macrophages requires the transcription factor NFAT5. *J Exp Med* 209(2):379–393.
4. Kim Y-M, Brinkmann MM, Paquet M-E, Ploegh HL (2008) UNC93B1 delivers nucleotide-sensing toll-like receptors to endolysosomes. *Nature* 452(7184):234–238.
5. Brinkmann MM, et al. (2007) The interaction between the ER membrane protein UNC93B and TLR3, 7, and 9 is crucial for TLR signaling. *J Cell Biol* 177(2):265–275.
6. Smolenski RT, Lachno DR, Ledingham SJ, Yacoub MH (1990) Determination of sixteen nucleotides, nucleosides and bases using high-performance liquid chromatography and its application to the study of purine metabolism in hearts for transplantation. *J Chromatogr A* 527(2):414–420.
7. Golding EM, Teague WE, Jr., Dobson GP (1995) Adjustment of K′ to varying pH and pMg for the creatine kinase, adenylate kinase and ATP hydrolysis equilibria permitting quantitative bioenergetic assessment. *J Exp Biol* 198(Pt 8):1775–1782.
8. Brouilette SW, et al.; West of Scotland Coronary Prevention Study Group (2007) Telomere length, risk of coronary heart disease, and statin treatment in the West of Scotland Primary Prevention Study: A nested case-control study. *Lancet* 369(9556):107–114.
9. Huggins A, Paschalidis N, Flower RJ, Perretti M, D'Acquisto F (2009) Annexin-1-deficient dendritic cells acquire a mature phenotype during differentiation. *FASEB J* 23(4):985–996.
10. D'Acquisto F, et al. (2007) Annexin-1 modulates T-cell activation and differentiation. *Blood* 109(3):1095–1102.

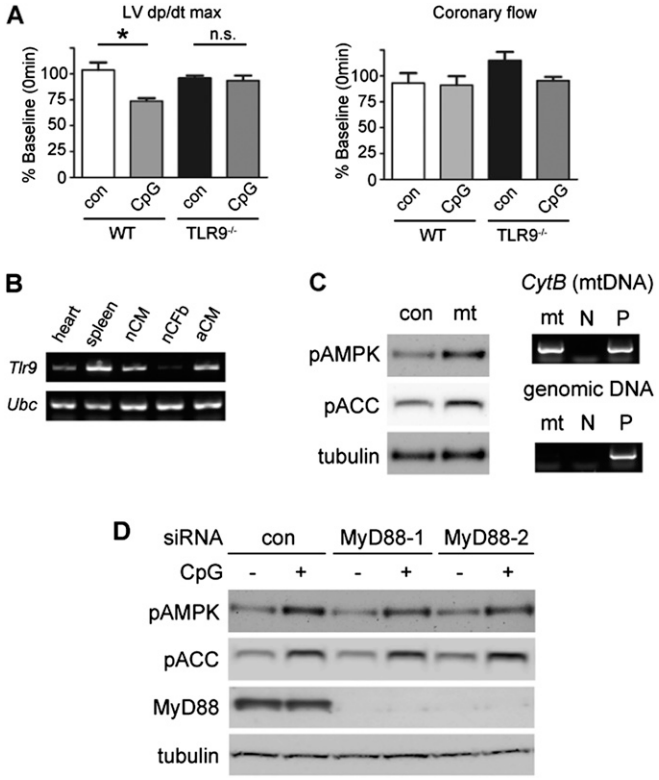

Fig. S1. Supporting data for Fig. 1. (*A*) CpG-ODN significantly decreased cardiac contractility (LV dp/dt max) through TLR9 without changing coronary flow. Percent changes from baseline at 30 min after the administration of CpG-ODN are shown. $n = 6$ (WT), and 5 ($TLR9^{-/-}$) for each group. Mean ± SEM, $^{*}P < 0.05$ vs. control vehicle group. NS, not significant. (*B*) Expression of *Tlr9* in rat primary cardiomyocytes. DNaseI-treated total RNA (1 μg) was subjected to conventional RT-PCR. *Ubiquitin C (Ubc)* was used for internal control. nCM, neonatal cardiomyocyte; cCFb, neonatal cardiac fibroblasts; aCM, adult cardiomyocytes. (*C*) Mitochondrial DNA (mt; 10 μg/mL) also activated AMPK in cardiomyocytes 60 min after administration. The data represent two independent experiments. The extracted mtDNA was positive for CytB (mitochondria DNA) but not for the genomic DNA (Tlr9 locus). P, positive control for each primer set; N, water. $^{*}P < 0.05$, $^{**}P < 0.01$, $^{***}P < 0.001$ compared with vehicle control. (*D*) Knockdown of Myd88 (MyD88-1 and MyD88-2) did not inhibit TLR9-mediated AMPK activation in rat neonatal cardiomyocytes. The data represent three independent experiments.

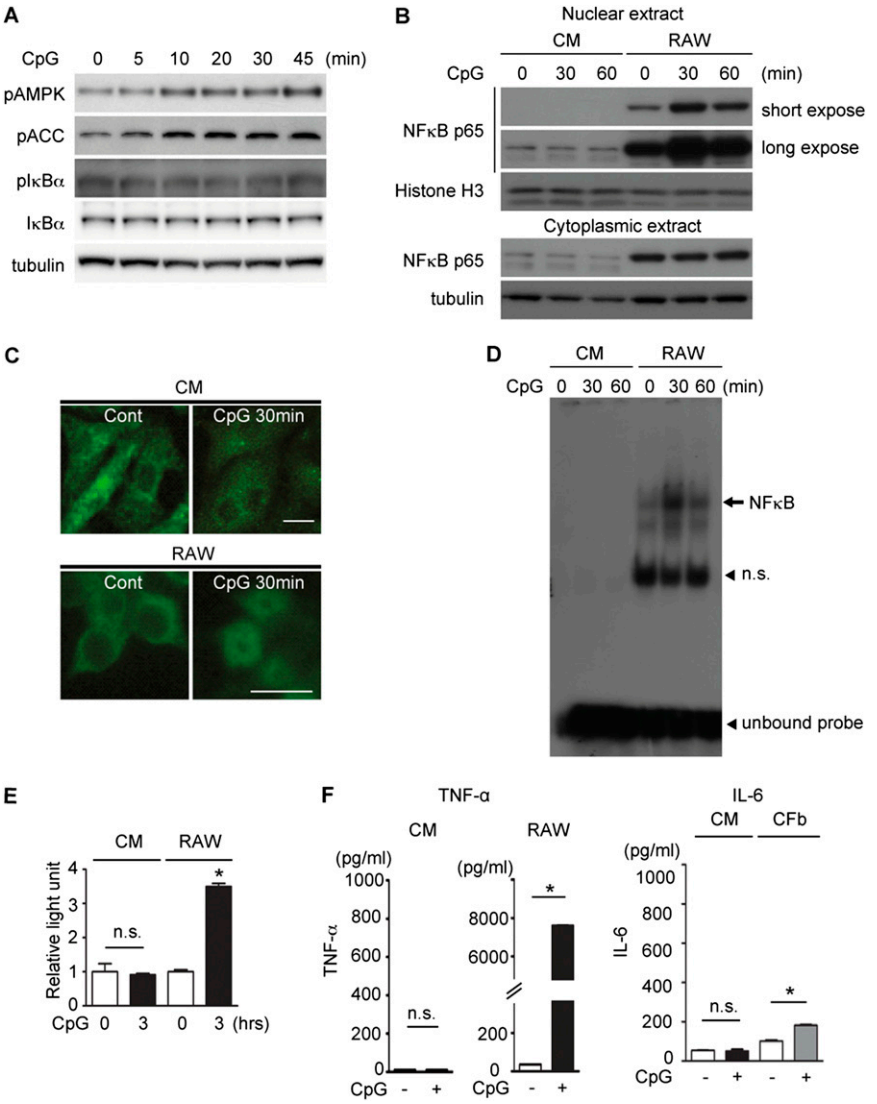

Fig. S2. Supporting data for Fig. 1. (*A*) CpG-ODN did not induce phosphorylation or degradation of IκBα in cardiomyocytes. Data represent two different experiments. (*B*) NF-κB p65 subunit in the nuclear fraction increased at 30 and 60 min after TLR9 stimulation in RAW264.7 cells (RAW), but not in cardiomyocytes (CM). Data represent three different experiments. (*C*) NF-κB p65 subunit translocated from the cytosol to the nucleus in RAW264.7 cells (RAW) assessed with immunofluorescence, but this was not observed in cardiomyocytes (CM). (Scale bars, 10 μm.) (*D*) Electrophoretic mobility shift assay showing NF-κB/DNA-binding activity increased after stimulation with CpG-ODN in RAW264.7 cells (RAW), but not in cardiomyocytes (CM). Data represent three different experiments. NS, nonspecific binding. (*E*) Luciferase assay demonstrated there was no increase in NF-κB transcriptional activity in cardiomyocytes (CM) at the indicated time points, in contrast to significant induction in RAW264.7 cells (RAW). ($n = 6$ for each group). Error bars indicate SEM. Data represent two different experiments. (*F*) CpG-ODN administration induced cytokine production (TNF-α and IL-6) in RAW264.7 cells (RAW) and cardiac fibroblasts (CFb), but not in cardiomyocytes (CM). Cells were treated with CpG-ODN (typeB; 3 μM) for 16 h ($n = 3$ for each group). Error bars indicate SEM. Data represent two different experiments. *$P < 0.05$ compared with the vehicle control.

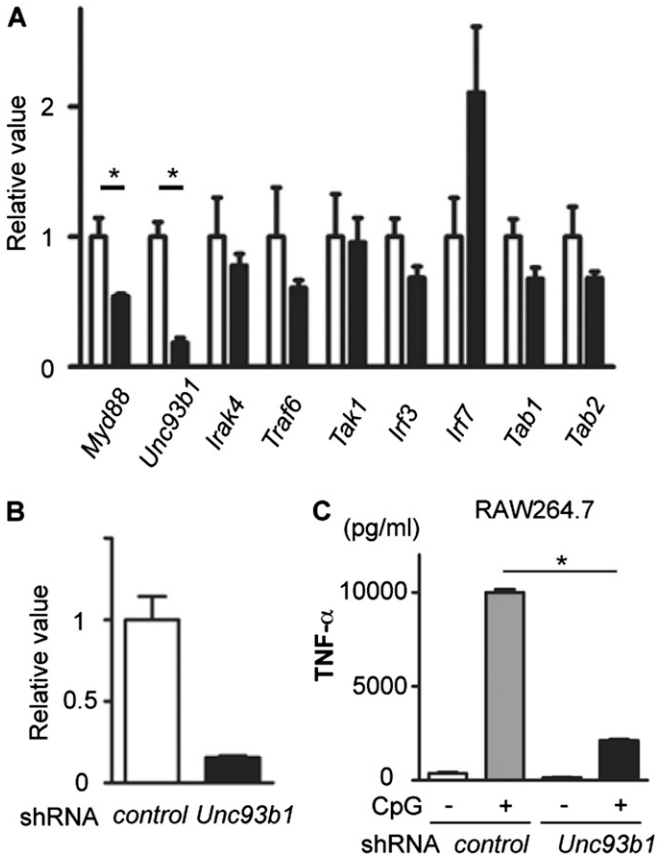

Fig. S3. Supporting data for Fig. 2. (*A*) Semiquantitative RT-PCR screening of TLR9 signaling molecules between RAW264.7 ($n = 3$) and mouse neonatal cardiomyocytes ($n = 5$). Unc93b1 was significantly less expressed in cardiomyocytes than in RAW264.7 cells. Comparison was made by *t* test with statistical difference accepted when $P < 0.05$. *$P < 0.05$ compared with RAW264.7 cells. (*B*) Validation of shRNA for *Unc93b1* in RAW264.7 cells. Expression of *Unc93b1* was measured by real-time PCR in RAW264.7 cells transfected with the control or shRNA specific for Unc93b1. (*C*) *Unc93b1* knockdown reduced inflammatory response. 2.5×10^5 of either control or *Unc93b1* shRNA-transfected RAW264.7 cells were plated in 24-well plates, then treated with CpG-ODN (typeB; 3 μM) for 2 h. Collected supernatant was measured by TNF-α ELISA. Error bars indicate SEM. $n = 3$ for each group. Data represent two different experiments. *$P < 0.05$.

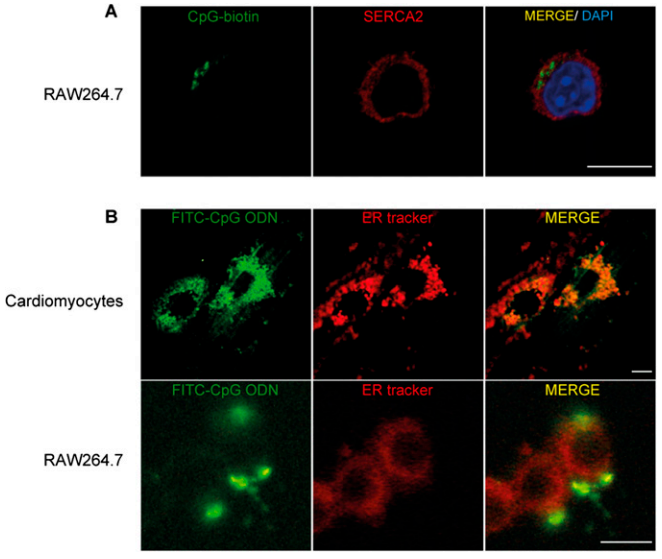

Fig. S4. Supporting data for Fig. 4. (*A*) Distribution of biotin-labeled CpG-ODN (green) in RAW264.7 cells were punctate pattern, which was different from the pattern in cardiomyocytes and did not merge with the ER marker (SERCA2; red) 30 min after administration. Images were obtained with confocal microscopy. (*B*) Endocytosed CpG-ODN localized in the ER in cardiomyocytes. Please note a different distribution pattern from that in RAW264.7 cells. Both cardiomyocytes and RAW264.7 cells were labeled with ER tracker dye (red), then incubated with FITC-labeled CpG-ODN1668 (3 μM) for 30 min. Images were obtained with fluorescent microscopy. (Scale bars, 10 μm.) Experiments were repeated at least twice and the representative images are shown.

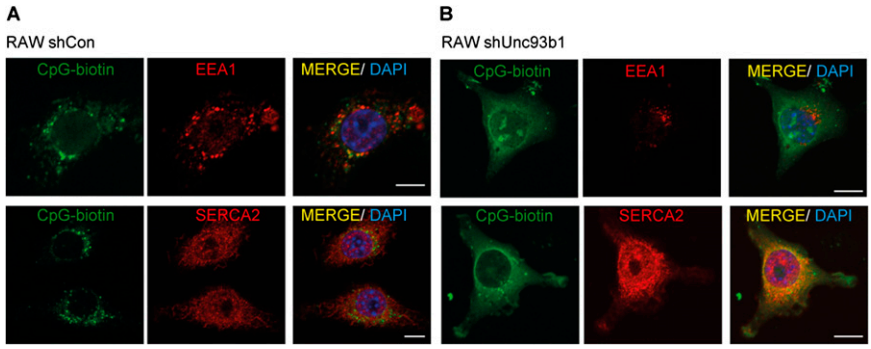

Fig. S5. Supporting data for Fig. 4. (*A*) The distribution of biotin-labeled CpG-ODN (green) in control RAW264.7 cells was punctate pattern. Endocytosed CpG-ODN merged with endosome marker, EEA1 (red; *Upper*), but did not merge with the ER marker (SERCA2; red, *Lower*) 30 min after administration. (*B*) In contrast, endocytosed CpG-ODN (green) became spread and less punctate in *Unc93b1* knocked-down RAW cells. Images were obtained with confocal microscopy. (Scale bars, 10 μm.) The data represent three different experiments and the representative images are shown.

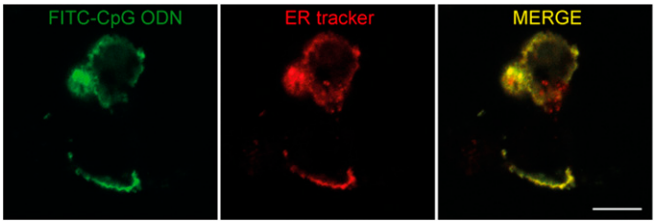

Fig. S6. Supporting data for Fig. 5. Endocytosed CpG-ODN localized in the ER in neuronal cells. Differentiated SHSY5Y cells were labeled with ER tracker dye (red), then incubated with FITC-labeled CpG-ODN1668 (3 μM) for 30 min as in Fig. S4*B*. (Scale bars, 10 μm.) Experiments were repeated at least twice and the representative images are shown.

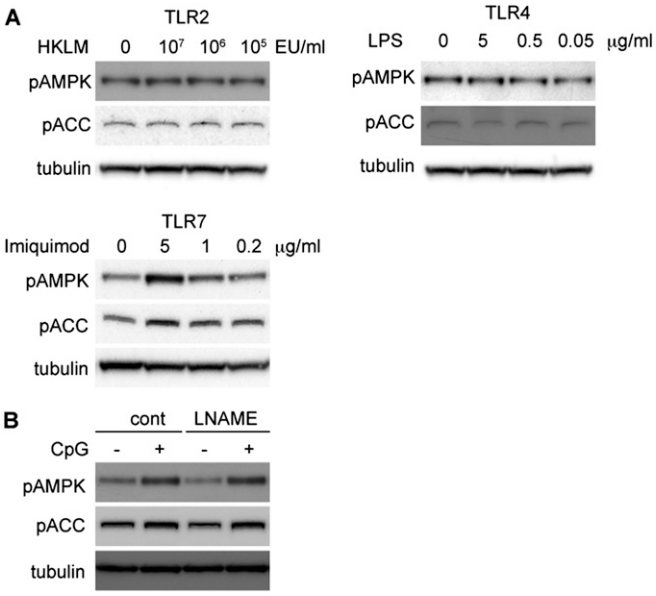

Fig. S7. (*A*) Although there was no AMPK activation at 60 min after TLR2 (HKLM) or TLR4 (LPS-EB) stimulation at the indicated concentrations, TLR7 stimulation (imiquimod) increased the phosphorylation level of AMPK. (*B*) Pretreatment with nonspecific NO synthase inhibitor, L-NAME (10^{-3} M, 30 min), did not inhibit the TLR9-mediated AMPK activation. Experiments were repeated at least twice and the representative images are shown.

Rat

	forward primer	reverse primer
Unc93b1	5′- GCCCTCTTCGTCTCTACCAA	5′- TCTGGGACATCCTGGTGATA
MyD88	5′- ACCAAGTTTGCTCTCAGCCT	5′- CGCAGATAGTGATGAACCGT
TLR9	5′- CTAGACGTGAGAAGCAACCCTCTG	5′- CAGCTCGTTATACACCCAGTCGGC
Ubc	5′- CGCTGACAATGCAGATCTTT	5′- CTTGTCCTGGATCTTTGCCT

Mouse

	forward primer	reverse primer
Unc93b1	5′- AACGCTACTACACGCTGGTG	5′- TCTGGGACATCCTGGTGATA
IRF3	5′- AGGAACAATGGGAGTTCGAG	5′- CAGTGTCATGTCAGCTGTGC
IRF7	5′- GAGCAAGACCGTGTTTACGA	5′- ATGATGGTCACATCCAGGAA
TRAF6	5′- GTGGAGTTTGACCCACCTCT	5′- TGCATCCCTTATGGATTTGA
MyD88	5′- TGGTGGTTGTTTCTGACGAT	5′- GGAAAGTCCTTCTTCATCGC
B2MG	5′- CCTTCAGCAAGGACTGGTCT	5′- TGTCTCGATCCCAGTAGACG
IRAK4	5′- TCAAGCCCAGACAACAGAAG	5′- GCTCGTCGAAGTTGTTTGTG
TAK1	5′- GTCCTCCTCCTCGTCTTCTG	5′- CTCTTCCGACAACCTCTTCC
TAB1	5′- CTGAGCACACTGAGGCTGAT	5′- TCTCAGCTAAGGCATCATCG
TAB2	5′- CCCAAAGATCAAAGGTCCAC	5′- CGAGGCATCTCACACTGTTC

Human

	forward primer	reverse primer
Unc93b1	5′- ACTACAAGGAGCAGGATGGG	5′- AAGCTCAGATGGAAGAAGCTG
TLR9	5′- CCAGCTACATCCCGATACCT	5′- GTTCTCACTCAGGTCCAGCA
Ubc	5′- TCTTGTTTGTGGATCGCTGT	5′- TCGAGGGTGATGGTCTTACC

Fig. S8. PCR primers used in this study.